IOP PUBLISHING PHYSICS IN MEDICINE AND BIOLOGY

Phys. Med. Biol. **52** (2007) 5603–5617 doi:10.1088/0031-9155/52/18/009

Tissue heterogeneity as a mechanism for localized neural stimulation by applied electric fields

P C Miranda[1], L Correia[1], R Salvador[1] and P J Basser[2]

[1] Institute of Biophysics and Biomedical Engineering, Faculty of Sciences, University of Lisbon, 1749-016 Lisbon, Portugal
[2] Section on Tissue Biophysics and Biomimetics, NICHD, National Institutes of Health, Bethesda, MD 20892-1428, USA

E-mail: pcmiranda@fc.ul.pt

Received 16 April 2007, in final form 27 June 2007
Published 3 September 2007
Online at stacks.iop.org/PMB/52/5603

Abstract

We investigate the heterogeneity of electrical conductivity as a new mechanism to stimulate excitable tissues via applied electric fields. In particular, we show that stimulation of axons crossing internal boundaries can occur at boundaries where the electric conductivity of the volume conductor changes abruptly. The effectiveness of this and other stimulation mechanisms was compared by means of models and computer simulations in the context of transcranial magnetic stimulation. While, for a given stimulation intensity, the largest membrane depolarization occurred where an axon terminates or bends sharply in a high electric field region, a slightly smaller membrane depolarization, still sufficient to generate action potentials, also occurred at an internal boundary where the conductivity jumped from 0.143 S m^{-1} to 0.333 S m^{-1}, simulating a white-matter-grey-matter interface. Tissue heterogeneity can also give rise to local electric field gradients that are considerably stronger and more focal than those impressed by the stimulation coil and that can affect the membrane potential, albeit to a lesser extent than the two mechanisms mentioned above. Tissue heterogeneity may play an important role in electric and magnetic 'far-field' stimulation.

1. Introduction

Neural stimulation using low frequency electric fields may be achieved through a variety of mechanisms. For long, straight, uniform unmyelinated fibres, the passive response of the axon to an applied electric field, $\vec{E}$, can be modelled in terms of the cable equation (Basser and Roth 1991, Roth and Basser 1990)

$$\lambda^2 \frac{\partial^2 V'}{\partial^2 x} - \tau \frac{\partial V'}{\partial t} - V' = \lambda^2 \frac{\partial E_x}{\partial x}, \tag{1}$$

0031-9155/07/185603+15$30.00

where $V' = V_m - V_r$ is the deviation of the transmembrane potential V_m from its resting value V_r, E_x is the component of the total electric field in the direction of the axon, and τ and λ are the membrane time and space constants, respectively. If, in the steady state, V' also varies slowly[3] with x then the first two terms on the left are negligible and $-\lambda^2 \frac{\partial E_x}{\partial x}$ provides an estimate of the change in membrane potential caused by the stimulus. Thus, the membrane is most strongly depolarized where $-\lambda^2 \frac{\partial E_x}{\partial x}$ is the largest, i.e. where the electric field is decreasing most rapidly, and therefore this is where an action potential is likely to be initiated. This term is usually referred to as the activating function. Here it has been written in terms of the electric field so that it applies to both electric and magnetic stimulation. In magnetic stimulation the electric field is generated by electromagnetic induction and is given by $\vec{E} = -\frac{\partial \vec{A}}{\partial t} - \nabla\phi$, where $\vec{A}$ and ϕ represent the magnetic vector potential and the electric scalar potential, respectively, (Roth *et al* 1991a). For electric stimulation, the activating function can be written as $\lambda^2 \frac{\partial^2 \phi}{\partial x^2}$ (Rattay 1986).

In general, however, axons may terminate, follow curved paths, branch, or change diameter. In these cases, membrane polarization can take place even in the absence of an electric field gradient (Tranchina and Nicholson 1986, Reilly 1989). For a straight fibre of finite length $L \gg \lambda$ in a uniform electric field, a significant polarization occurs only in the vicinity of the termination, with a maximum magnitude λE_x at the termination point (Roth 1994). The polarity of the change in membrane potential depends on whether the electric field is directed into (hyperpolarization) or out of (depolarization) the axon membrane at the termination. For curved fibres with sharp bends, the membrane polarization at the bend is proportional to λE_x and a membrane polarization proportional to $\bar{\lambda} E_x$ is also predicted for sudden changes in the axon diameter, where $\bar{\lambda}$ is a function of the space constants on either side of the discontinuity in diameter (Roth 1994). Stimulation at terminations and bends is likely to be particularly relevant in the brain (Nagarajan *et al* 1993, Maccabee *et al* 1993).

In this paper we investigate the possibility that tissue heterogeneity may also affect significantly the transmembrane potential of excitable cells, even when they are subjected to an applied electric field whose amplitude may be uniform on the scale of the membrane space constant. Indeed, tissue heterogeneity can introduce large local changes in the spatial distribution of both the electric field and the electric field gradient, due to charge accumulating at the boundaries separating tissues with different electrical conductivities. Charge builds up at tissue boundaries whenever the normal component of the applied electric field is not zero and gives rise to a secondary electric field that ensures the continuity of the normal component of the current density.

Charge accumulation at the tissue–air boundary during magnetic stimulation has already been shown to reduce the normal component of the current density in the volume conductor to zero (Tofts 1990, Branston and Tofts 1991, Roth *et al* 1991b, Heller and van Hulsteyn 1992) and its effect is taken into account in most studies. However, few studies have sought to quantify the effect of internal boundaries on the electric field distribution. Some authors have investigated experimentally the effect of a soft tissue–bone interface on the magnetic stimulation of peripheral nerves (e.g., Maccabee *et al* (1991), Schmid *et al* (1992)), while others have modelled numerically the effect of interfaces between different soft tissues (e.g., Kobayashi *et al* (1997), Liu and Ueno (2000), Miranda *et al* (2003)).

Another consequence of tissue heterogeneity, hitherto unexplored, is its local effect on the membrane potential of an axon that crosses an internal boundary, such as a white-matter-grey-matter interface. The accumulation of charge at the boundary gives rise to a discontinuity in the normal component of the electric field, whose magnitude is given by $\Delta E_n = 2\nabla\phi$, where

[3] By 'slowly' we mean that $V'(x)$ varies over spatial wavelengths much greater than the membrane's space constant.

ϕ is the electric potential due to the surface charge accumulated on the boundary. The electric field at the interface is depressed in the high conductivity region by $\nabla\phi$ and is boosted in the low conductivity region by the same amount. The amplitude of this discontinuity is related to the normal component of the total electric field at the boundary, $\vec{E}$, by

$$\Delta E_n = 2\left(\frac{\sigma_1 - \sigma_2}{\sigma_1 + \sigma_2}\right)\vec{E}\cdot\vec{n}, \tag{2}$$

where $\sigma_1(\sigma_2)$ is the electrical conductivity of the tissue anterior (posterior) to the interface, as determined by the direction of the electric field (Miranda *et al* 2003). If the jump in the normal component of the electric field is modelled as a Heaviside step function of height ΔE_n then the derivative of the electric field along the direction of the axon (x) is a Dirac delta function, $\Delta E_x\delta(x)$, and the cable equation for a long, straight unmyelinated axon can be written as

$$\lambda^2\frac{\partial^2 V'}{\partial^2 x} - \tau\frac{\partial V'}{\partial t} - V' = \lambda^2\Delta E_x\delta(x), \tag{3}$$

where $\Delta E_x = \Delta E_n\cos(\theta)$, θ being the angle between the interface normal and the axon's axis. The steady-state solution for this equation is

$$V'(x) = -\frac{\lambda\Delta E_x}{2}\mathrm{e}^{-\frac{|x|}{\lambda}} \tag{4}$$

assuming again that $L \gg \lambda$. See Plonsey and Barr (2000, p 186) for the solution to a similar problem. At the location of the electric field jump, $x = 0$, the change in membrane potential is given by $\lambda\Delta E_x/2$.

In this paper we examine the relative importance of the above-mentioned neural stimulation mechanisms by comparing the magnitude of the changes in membrane potential due to the electric field, λE_x, to the electric field gradient, $\lambda^2\frac{\partial E_x}{\partial x}$, and to the electric field discontinuity, $\lambda\Delta E_x/2$, in different situations. In all cases the electric field is induced by a magnetic stimulator with a figure 8 coil.

2. Methods

2.1. The axonal length constant

Some knowledge of the axonal length constant, λ, is required to compare the changes in membrane potential caused by the different stimulation mechanisms. For myelinated axons the length constant will have different values in the myelinated sections and in the nodes of Ranvier. Basser (1993) derived a macroscopic cable equation for a composite myelinated axon and calculated the macroscopic (or equivalent) length constant to be 2.08 mm for an axon of 14 μm in outer diameter. This result is in broad agreement with Hursh's cat data showing the internodal distance to be about 1 mm for 10 μm outer diameter axons (Hursh 1939), combined with the notion that λ should be similar to or greater than the internodal distance. In the human motor cortex, the largest cells are the pyramidal Betz cells in layer V, which have axons with outer diameters in the range of 10–20 μm (Lassek 1940, 1942). Since the axons with larger diameters are those with lower stimulation thresholds (Basser and Roth 1991, Fang and Mortimer 1991), we have assumed an axon outer diameter of 10 μm and taken $\lambda = 2$ mm in our calculations.

2.2. The stimulation coil

The coil used in these calculations replicates Magstim's 70 mm double coil, as described by Thielscher and Kammer (2002). It has two circular wings with nine turns each, whose

radii are given by $r_i = 26.5 + 2.125i$ mm, $i = 0$ to 8, with a 90 mm separation between the wing centres. In the first two calculations, the maximum rate of change of the current was set to 67 A μs^{-1}. This corresponds to the average motor threshold for a monophasic impulse using this coil with the Magstim 200 stimulator to induce a posterior–anterior current in the brain (Thielscher and Kammer 2002, Kammer *et al* 2001). In the third calculation, the stimulus intensity was specified by setting the stimulator's capacitor voltage to 1000 V, which corresponds to a maximum current rate of change of 61.2 A μs^{-1}. Values of the electric field, the electric field gradient and the change in membrane potential at other stimulus intensities can be obtained by linearly scaling the values presented here.

2.3. The volume conductor model

A spherical head model with a radius of 92 mm (Rush and Driscoll 1969) was used in the first two calculations. In this model, the surface of the sphere corresponds to the scalp and the spherical surface with a radius of 80 mm corresponds to the surface of the brain. The sphere is centred on the origin of the coordinate system. The coil is positioned in the plane $z = 102$ mm, tangential to the sphere. The line passing through the centre of both wings is aligned parallel to the x-axis; under the centre of the coil the induced electric field points along the y-axis.

In the third calculation, the volume conductor was a rectangular hexahedron with dimensions $(x, y, z) = 40 \times 60 \times 17.5$ cm^3 divided in half with different electrical conductivities. The large dimensions of the hexahedron ensured that charge accumulation on its outer boundaries had a negligible effect on the electric field in the vicinity of the internal interface. One half ($y = -30$ to 0 cm) had an electrical conductivity of 0.143 S m^{-1}, the other half ($y = 0$ to 30 cm) had an electrical conductivity of 0.333 S m^{-1}. These values are representative of the conductivities of white matter and grey matter, respectively, (Haueisen *et al* 1997). The coil was placed 5 mm above and parallel to the conducting media with its centre directly above the centre of the internal boundary. The orientation of the coil and the direction of current flow in its windings were such that the electric field induced under the centre of the coil pointed along the positive y-axis, perpendicular to the internal boundary. A 6 cm line segment representing the axon was placed parallel to the y-axis, 3.0 cm below the coil's centre. The direction of the applied electric field was chosen so as to depolarize the axon end in the higher conductivity region.

2.4. Calculations in the homogeneous spherical head model

For the homogeneous spherical head model the total induced electric field, $\vec{E} = -\frac{\partial \vec{A}}{\partial t} - \nabla\phi$, was calculated using Eaton's formulae (Eaton 1992) implemented in Mathematica (Wolfram Research, Inc., http://www.wolfram.com). The Cartesian components of the electric field were computed on a grid of 11×11 points lying on a spherical surface of radius 77 mm, which corresponds approximately to 3 mm below the cortical surface (Roth *et al* 1991b). The points were separated by an arc length of exactly 1 cm along the y-direction and by 1 cm or slightly less along the x-direction.

The components of the electric field gradient tensor are

$$\nabla\vec{E} = \begin{pmatrix} \frac{\partial E_x}{\partial x} & \frac{\partial E_x}{\partial y} & \frac{\partial E_x}{\partial z} \\ \frac{\partial E_y}{\partial x} & \frac{\partial E_y}{\partial y} & \frac{\partial E_y}{\partial z} \\ \frac{\partial E_z}{\partial x} & \frac{\partial E_z}{\partial y} & \frac{\partial E_z}{\partial z} \end{pmatrix}. \tag{5}$$

They were estimated at a given point in the grid by computing the electric field components at six neighbouring points displaced by ±1 mm along each axis. For a given direction specified by a vector $\vec{n}$, the magnitude of the net electric field gradient along that direction is given by $\vec{n}^T(\nabla\vec{E})\vec{n}$. Note, only the symmetric part of the tensor, $(\nabla\vec{E} + (\nabla\vec{E})^T)/2$, contributes to this projection. We will refer to this scalar quantity as the directional derivative of the electric field. The orientation that maximizes the magnitude of directional derivative is given by the eigenvector associated with the largest eigenvalue of the symmetric part of the electric field gradient tensor. The electric field calculations were also performed using the finite element method (see below) to cross validate the results.

2.5. Calculations in the heterogeneous spherical head model

For the heterogeneous spherical head model, a cylindrical inclusion was placed below the coil centre with its axis parallel to the y-axis, in the plane $z = 72$ mm. The base of the cylinder mimics a vertical wall in a sulcus and the cylinder axis is 20 mm below the scalp. The length of the cylinder extended from $y = -5$ mm to $y = +5$ mm, with a radius of 5 mm. The electric conductivities of the sphere and the cylinder were taken to be 0.333 S m^{-1} (approximately that of grey matter (Haueisen *et al* 1997)) and 1.79 S m^{-1} (that of cerebrospinal fluid (Baumann *et al* 1997)), respectively. In this configuration (see the inset in figure 4) and near the centre of the cylinder bases, only the component of the electric field parallel to the cylinder axis, E_y, is significantly affected by the heterogeneity. In order to estimate $\frac{\partial E_y}{\partial y}$ just outside the centre of the cylinder base, a second degree polynomial was fitted to the electric field data in the homogeneous sphere (dashed curve in figure 4) and an exponential curve was fitted to the difference in the electric field introduced by the inclusion. The sum of the two fitted curves was then differentiated to obtain the slope of the solid curve in figure 4. The electric field distribution was calculated using a commercial finite element package (Comsol 3.2b with the electromagnetics module, http://www.comsol.com/) and a frequency of 5 kHz was chosen for the time-harmonic analysis.

2.6. Calculations involving the electric field discontinuity

The change in membrane potential where the axon crosses a boundary separating tissues with different electrical conductivity values is given by $\lambda\Delta E_x/2$ for unmyelinated axons. This effect, however, may be significantly different for myelinated axons, since the electric field varies rapidly with distance from the boundary and it may not be appropriate to use homogenized values for λ and τ in (3). Thus, in order to assess the effect of the electric field discontinuity on the membrane potential of a myelinated axon more faithfully, a model of the axon was implemented in which the axon is described as a sequence of compartments. In this model, a single compartment representing a node of Ranvier separates series of ten compartments representing the myelinated sections, of length L, from each other. For each point of the discretized axon, the compartmental cable equation is (Nagarajan *et al* 1993)

$$C_m\frac{\mathrm{d}V(n)}{\mathrm{d}t} + I_{\mathrm{ionic},n} - G_a(V(n+1) - 2V(n) + V(n-1)) = -G_a\left(\int_{nL}^{(n+1)L}(\vec{E}\cdot\vec{s})\,\mathrm{d}s - \int_{(n-1)L}^{nL}(\vec{E}\cdot\vec{s})\,\mathrm{d}s\right), \tag{6}$$

where C_m is the membrane capacitance, $V(n)$ is the transmembrane potential at the nth point of the discretized axon, $I_{\mathrm{ionic},n}$ is the membrane ionic current at the nth point, G_a is the axial conductance and $\vec{E}\cdot\vec{s}$ is the projection of the applied electric field along the axon. The

expression for the electric field, $\vec{E}$, must include both the magnetic vector potential term and the gradient of the external electric potential (Nagarajan and Durand 1996). In (6), the value of the membrane capacitance as well as the expression for the membrane ionic current depend on whether the point corresponds to a myelinated section or to a node of Ranvier. For myelinated sections, the membrane is described by a passive model consisting of a parallel RC circuit (Basser 2004). The membrane in each node of Ranvier is described by an active nonlinear model based on data from the rabbit's myelinated axon (Warman *et al* 1992). In the first and last points of the discretized axon, sealed end boundary conditions were implemented (Nagarajan *et al* 1993). The resulting set of equations was solved using the Picard iterative procedure (Mascagni and Sherman 1998). The numerical computations were performed using Matlab (Matlab 7.0, The MathWorks, http://www.mathworks.com/).

The electric field calculations were performed using a finite element package, as described in the previous subsection. Two hundred electric field values, equally spaced along the axon, were exported to a file. Interpolation of these values was achieved by fitting a combination of fifth-order polynomials and Heaviside functions to the exported data.

In this calculation the stimulus waveform must be taken into account so the Magstim 200 (Jalinous 1991) was modelled as a series RLC circuit ($L = 16.35$ μH, $C = 185$ μF, $R = 0.05$ Ω) until the time rate of change of the current in the coil, $\mathrm{d}i/\mathrm{d}t$, reaches the first minimum. After that, the circuit was modelled as a series LR circuit ($L = 16.35$ μH, $R = 0.088$ Ω). The resulting $\mathrm{d}i/\mathrm{d}t$ waveform was monophasic, with characteristics similar to those of the pulse generated by the Magstim 200 stimulator with the 70 mm double round coil (rise time = 82.1 μs, ratio of negative to positive peak amplitudes of $\mathrm{d}i/\mathrm{d}t$ curve = 0.25).

2.7. Quasistatic approximation

In all calculations, the contribution of the induced electric field to the total magnetic field was not taken into account. It is known to be negligible because of the low frequencies involved in trancranial magnetic stimulation (TMS), <5 kHz, and the low conductivity of brain tissues, about 1 S m^{-1} (Eaton 1992, Roth *et al* 1991a). In the results, electromagnetic wave propagation effects were found to be absent, in agreement with the wavelength associated with the TMS stimulus being several orders of magnitude larger than the dimensions of the model. The relative permittivity of all tissues was 10^4: as expected from the high conductivity to permittivity ratio and the low frequencies involved, the tissues responded as if they were purely resistive.

3. Results

The magnitude and direction of the electric field induced in a homogeneous spherical volume conductor are shown in figure 1. The electric field strength is greatest under the centre of the coil where it reaches 88.1 V m^{-1} for a current rate of change of 67 A μs^{-1}, 15 mm below the scalp. The corresponding value of λE is 176 mV for $\lambda = 2$ mm.

The electric field's directional derivative at one of the grid points is best visualized by plotting its magnitude as a function of angle, as shown in figure 2. This plot corresponds to one of the two grid points where the directional derivative has its largest value, and is located 2 cm behind the coil centre, measured on the surface of the 77 mm radius sphere. The most negative value of the directional derivative occurs in the yz plane, along a direction 222° anticlockwise from the y-axis (lower left lobe in figure 2). It amounts to -1896 V m^{-2}, which corresponds to a value of 7.6 mV for the activation function. The ratio of the activating function to the λE term is 4.3%, and is independent of the rate of change of the current. A second set of

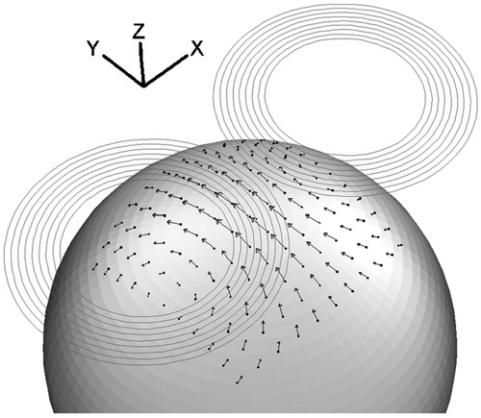

Figure 1. Plot of the electric field vector on a grid of 11 × 11 points on a spherical surface of radius 77 mm, 15 mm below the scalp surface and 25 mm below the coil. The arrows are tangential to the spherical surface.

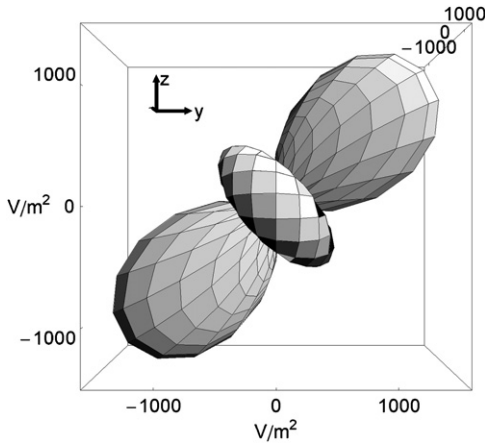

Figure 2. Polar plot showing the magnitude of the directional derivative of the electric field as a function of angle, at the second grid point behind the coil centre. The top right lobe points approximately towards the centre of the coil.

smaller lobes (+1276 V m^{-2}) points along the x-axis, in and out of the paper. The smallest lobes point perpendicularly to the first two sets and are not visible from this viewpoint. The spatial variation of the directional derivative on the 77 mm radius sphere is shown in figure 3, in the xz plane (a) and in the yz plane (b).

As for the heterogeneous model, the position of the high conductivity cylinder relative to the scalp and the coil is shown in the inset of figure 4. The plot shows the variation of the component of the electric field parallel to the cylinder axis, E_y, as a function of position along that axis, both for a homogeneous sphere (dashed curve) and with the cylindrical inclusion (solid curve). The other components of the electric field are negligible. At the boundary, outside the inclusion, the estimated values for E_y and $\frac{\partial E_y}{\partial y}$ are 99.5 V m^{-1} and 6051 V m^{-2}, respectively. Assuming that $\lambda = 2$ mm, the corresponding values of λE_y and $\lambda^2 \frac{\partial E_y}{\partial y}$ are 199 mV and 24.2 mV, respectively. The ratio of the activating function to the λE term is 12.2%.

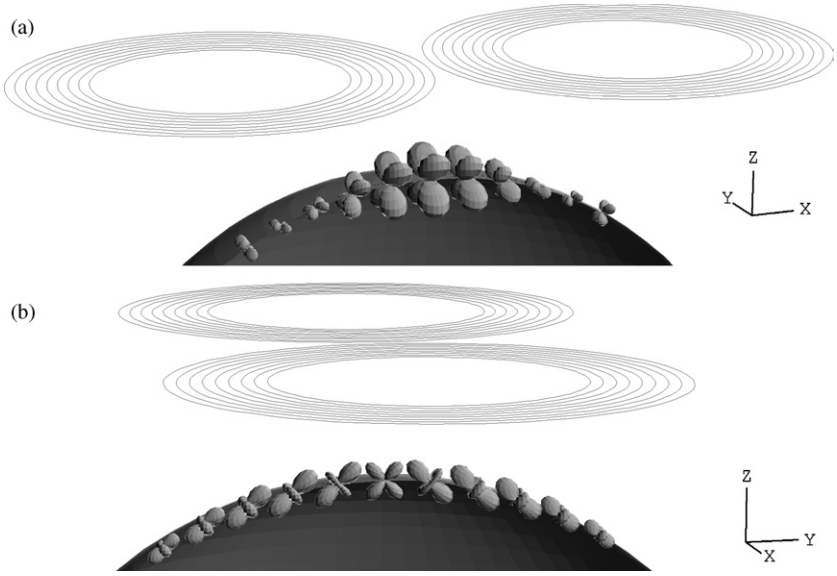

Figure 3. Polar plots of the electric field's directional derivative at 11 points on a spherical surface of radius 77 mm (a) along the x-axis and (b) along the y-axis. The polar plot in figure 2 is the fourth from the left in (b).

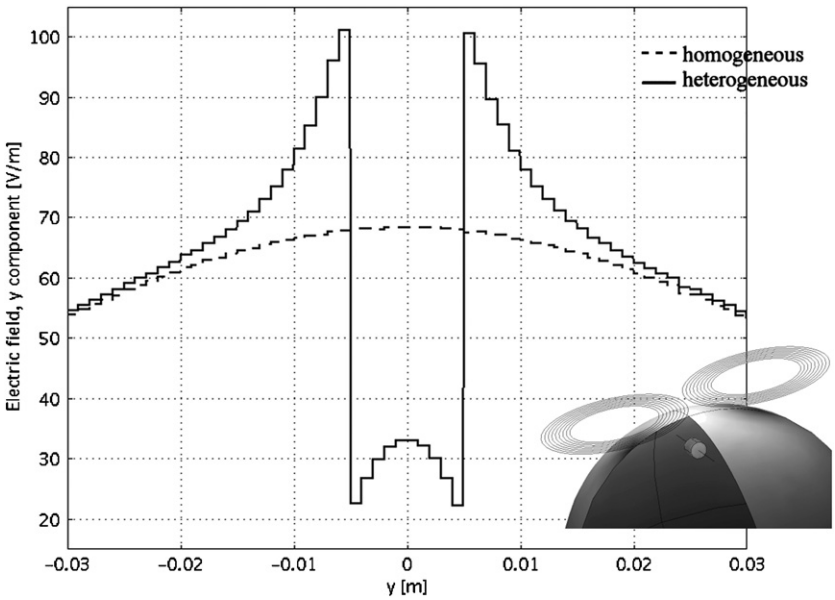

Figure 4. Plot of the component of the electric field parallel to the cylinder axis, E_y, as a function of position along that axis for a homogeneous sphere (dashed curve) and a heterogeneous sphere (solid curve). Inset: position of high conductivity cylindrical inclusion, showing the segment of the cylinder axis along which data are plotted, 30 mm below the plane of the coil.

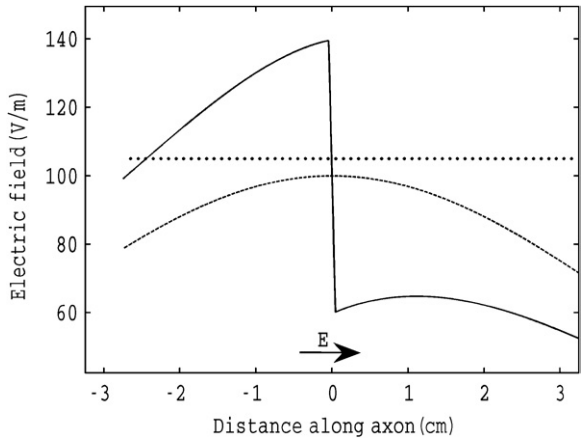

Figure 5. Plot of the axial component of the electric field along a straight axon as it passes at right angles through an interface between tissues whose conductivity values are 0.143 S m^{-1} to the left and 0.333 S m^{-1} to the right (solid curve) and for a homogeneous medium (dashed curve). The straight line shows the positions of the nodes of Ranvier on a 6 cm long axon, which is placed 30 mm below the plane of the coil.

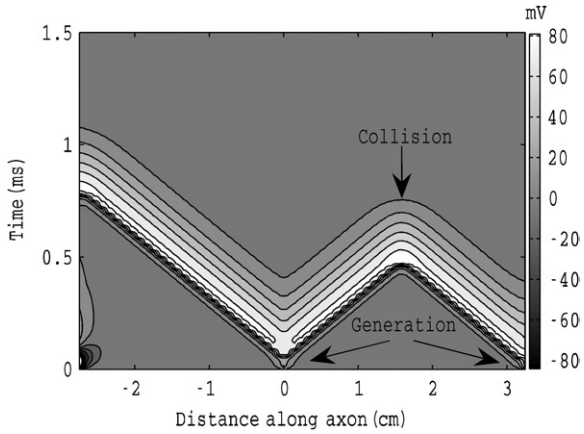

Figure 6. Contour plot of the membrane potential, V', as a function of position and time showing the generation and propagation of action potentials. An action potential is initiated at the middle of the axon by the electric field discontinuity and at the right end of the axon by the electric field. The left end of the axon is hyperpolarized at $t = 0$. As the two action potentials collide, propagation ceases.

The axial component of the induced electric field along a straight axon that crosses an interface between two tissues with different conductivities is shown in figure 5. The value of the electric field jump at the interface, ΔE_y, is 79.5 V m^{-1} (solid curve) and the value of the electric field E_y in the homogeneous medium at the same position is 100.4 V m^{-1} (dashed curve), in good agreement with (2). The electric field strength at the right axon end is 52.4 V m^{-1}.

The effect of this electric field distribution on the transmembrane potential is shown in figure 6. Action potentials are generated at the electric field discontinuity and at the axon end that undergoes depolarization (right end), but not at the axon end that undergoes

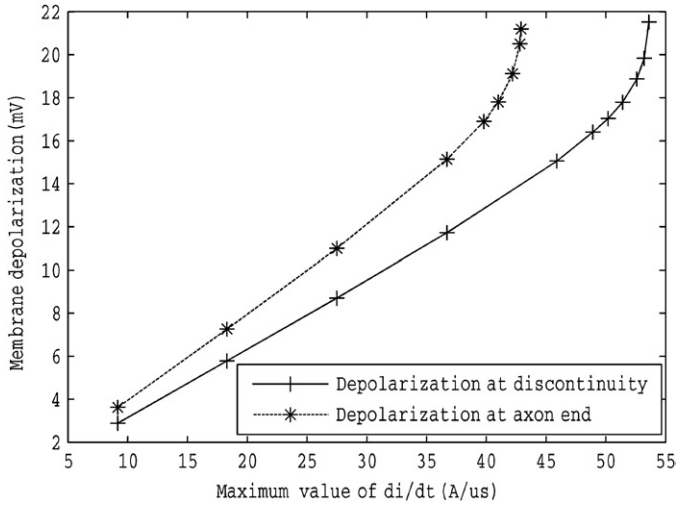

Figure 7. Subthreshold change in membrane potential V' as a function of stimulus intensity di/dt. The change is greatest at the axon end (dashed line) meaning that the threshold for stimulation is still lower there than at the electric field discontinuity (solid line).

hyperpolarization (left end). With time the action potentials propagate away from the point of origin. As they collide, on the right half of the axon, propagation ceases due to the refractory state in which the portion of the membrane ahead has been left. The contours in the rising edge of the action potential are so close together that they appear as an almost solid black strip. The value of $\lambda \Delta E_y/2$ is 79.5 mV, the value of λE_y at the depolarised axon end is 104.8 mV and their ratio is 0.76.

Figure 7 shows the rise in membrane potential as a function of stimulation intensity, expressed as the rate of change of current in the coil (A μs^{-1}), at the two points where stimulation occurs. The curve corresponding to the axon end rises faster than that for the electric field discontinuity, indicating that the threshold for stimulation is lower at the axon end (43.0 A μs^{-1}) than at the discontinuity (53.6 A μs^{-1}). The ratio of these thresholds is 0.80.

4. Discussion

The calculations of the electric field and the electric field gradient induced in a homogeneous sphere show that the electric field and its directional derivative have their largest amplitudes at different locations and along different directions. Even when these differences are taken into account the activation function has a considerably smaller maximum value than λE. This is not unexpected since if we take the electric field derivative to be approximately given by the maximum electric field divided by the radius, R, of the coil then the ratio of the gradient to the electric field terms is approximately λ/R (Roth 1994). If $\lambda = 2$ mm and $R = 50$ mm, this ratio is 4%.

In this paper we have introduced the idea of calculating the electric field gradient tensor and its projection along a specific direction. The results shown in figures 2 and 3 reveal the highly anisotropic nature of the directional derivative of the induced electric field, whose angular dependence is far from intuitive. They suggest that if a figure 8 coil is placed tangentially on the scalp with the induced electric field under the coil centre perpendicular to a cortical sulcus

then the directional derivative will be most negative along pyramidal cells that lie on the lip of the sulcus, halfway between the sulcus and the gyrus, perpendicular to the cortical surface. The axons of the pyramidal cells on the lip bend gently as they extend into the white matter so the electric field gradient mechanism may be the dominant mechanism for their stimulation, but this is only likely to occur at high stimulus intensities. In the situation shown in figure 2, the gradient component that is usually considered, $\frac{\partial E_y}{\partial y}$, is 2.5 times smaller than the maximum directional derivative. Thus, in peripheral nerve stimulation or other cases where the electric field gradient may be the principal stimulation mechanism, calculations of the directional derivative using appropriate models for the volume conductor may be useful to optimize the experimental protocol.

The main conclusions to be drawn from the results obtained with the heterogeneous model is that interfaces introduce strong local gradients compared to the homogeneous model (figure 4) and that the direction of the local gradient is also determined by the orientation of the interface, not only by the coil's configuration. Even so, the ratio of the maximum values of the activation function and of λE remains small. In this particular case, $\frac{\partial E_y}{\partial y}$ is the largest gradient component, unlike what was seen in the homogeneous case (figure 2). Again, these considerations may be relevant in situations where the electric field gradient is the main stimulation mechanism.

The discontinuous curve in figure 4 also demonstrates the influence of charge accumulating on nearby interfaces on the electric field and electric field gradient at or near the interface of interest: the electric field halfway between the two interfaces does not approach its homogeneous medium value; the electric field jump at the boundaries is no longer symmetric about its homogeneous value; it is slightly smaller than expected for a single interface; and the gradients, particularly in the inner region, are slightly reduced. These effects indicate that when modelling stimulation in a cortical sheet it is important to represent the various neighbouring interfaces, particularly in sulci when magnetic stimulation is being used.

The last set of calculations presented here confirms that an abrupt change in tissue conductivity can give rise to an action potential in a myelinated axon, even when the difference in electrical conductivities is modest and the boundary is positioned between two nodes of Ranvier (figure 5). In the case shown, the stimulation threshold is lower at the right axon end than at the discontinuity because $\lambda \Delta E_y/2$ is smaller than λE_y at that termination. The ratio of these two quantities (0.76) is a reasonable, but not completely accurate, predictor of the ratio of thresholds at these two locations (0.80).

At a real white-matter-grey-matter interface, an infinite conductivity gradient such as that modelled above is unlikely but a fairly steep one may exist. In transcranial electric or magnetic stimulation, bulk tissue conductivity is determined by the conductivity of the extracellular volume (Tuch *et al* 2001), where ion flow is restricted mostly by the presence of cell membranes and myelin. Even though this volume is continuous across the boundary separating these two tissues, the cellular arrangement and composition in each tissue is different, giving rise to different bulk conductivity values. However, at the microscopic level a conductivity gradient may exist corresponding to a gradient in cellular arrangement and composition. Thus the secondary electric field produced by charge accumulation at the boundary may be slightly smaller than that predicted in (2).

A comparison of the values obtained for λE_x, $\lambda^2 \frac{\partial E_x}{\partial x}$ and $\lambda \Delta E_x/2$ in the three conditions studied in this paper shows that the electric field term is the largest in all cases, indicating that the lowest threshold mechanism is likely to occur when axons end or bend in regions where the electric field has a strong component in the direction of the axon. When the axon's resistance to ionic flow along the direction of the applied electric field does not change sharply,

the lowest threshold mechanism is the existence of an abrupt change in tissue conductivity along the path of the axon in the presence of a high electric field component perpendicular to the boundary. In general, at an internal boundary and using (2)

$$\frac{\lambda \Delta E_n/2}{\lambda E_n} = \frac{\sigma_1 - \sigma_2}{\sigma_1 + \sigma_2}. \tag{7}$$

For the values of conductivity used in figure 5, this ratio is 0.40. Because this ratio is close to 1, the existence of an internal boundary may affect significantly the spatial distribution of the membrane potential, even in the presence of axon ends or bends, pulling the stimulation site closer to or pushing it further away from that boundary. The electric field gradient term was always the smallest, but it can be significantly enhanced by tissue heterogeneity.

The magnitude of the effects of tissue heterogeneity on the electric field distribution depends on the angle between the applied electric field and the boundary normal. Thus, tissue heterogeneity may introduce an extra directional dependence to the stimulation efficacy, in addition to that due to the relative orientation of the applied electric field and the neuronal structures (Rushton 1927).

5. Conclusions

We have shown that the jump in the normal component of the electric field at a boundary causes a change in membrane polarization of amplitude $\lambda \Delta E_x/2$ in an unmyelinated axon that crosses that interface at right angles. This amplitude is analogous to the one that arises at an axon termination, λE_x, with the magnitude of the electric field jump replacing the electric field strength. The factor of $1/2$ arises because the current injected into the intracellular space at the boundary splits in equal proportions to the right and to the left of the boundary. A similar situation occurs at a jump in the fibre radius or in intracellular conductivity, which gives rise to a change in the transmembrane potential of the form αE_x (Roth 1994), where α is a constant determined by the membrane properties on both sides of the discontinuity. In this respect, changes in macroscopic tissue properties can produce similar effects to those produced by changes in cellular or intracellular properties.

Our results support the suggestion that 'discontinuities in the geometry of the neuronal structure and the presence of inhomogeneities in the volume conductor can be more important in characterizing excitation rather than the field gradients' (Nagarajan *et al* 1993). We further suggest that the discontinuity in the electric field that occurs at internal boundaries across which the electrical conductivity changes abruptly may be a powerful mechanism for stimulating neurons that cross that boundary. Specifically, this work extends our notion of the 'activating function' to include the electric field discontinuity that arises from charge accumulation at internal boundaries. More generally, it highlights the importance of tissue heterogeneity as a mechanism for localized neural stimulation by applied electric fields.

The various effects of tissue heterogeneity were illustrated here using very simple boundary shapes. Obviously, similar effects will also be present in more realistic models of the head based on MR images (e.g., Kowalski *et al* (2002), Holdefer *et al* (2006), Wolters *et al* (2006)), which are necessary to obtain more accurate descriptions of the spatial distribution of the electric field in the brain. Our results provide a detailed understanding of the effects of tissue heterogeneity that permits a well-informed interpretation of the results obtained using these complex head models. Additionally, the results emphasize the importance of the correct representation of the surfaces separating tissues with different conductivities in such models.

Variations in electrical conductivity will similarly affect the distribution of the electric field produced in electrical stimulation. Just as in magnetic stimulation, the requirement

of current continuity in the static or quasistatic regime leads to the accumulation of charge at internal boundaries, causing electric field discontinuities at the boundaries and locally enhanced electric field gradients. Such effects may play an important role in transcranial direct current stimulation (tDCS).

The realization of tissue heterogeneity as a new source of neural excitation has potentially important consequences to TMS in particular, and to understanding the interaction of electric fields and tissue, in general. First, differences in electrical conductivity among grey matter, white matter and cerebrospinal fluid alone could result in depolarization or hyperpolarization of excitable tissues at or near interfaces between them. This mechanism of activation thus could provide a possible explanation for the observation of 'far-field' stimulation of brain and other tissues. Thus even a time-varying magnetic field whose magnetic vector potential is approximately spatially uniform within the brain could cause excitation by this mechanism, even in the absence of axon terminations or sharp bends. So, for example, this mechanism could be implicated in explaining the recent finding that Echo Planar MRI of brain can effect a mood change in normal subjects (Rohan *et al* 2004). Such an apparent TMS-like effect from switched magnetic field gradients is not expected using a conventional 'activating function'.

Second, models, such as the one presented here, could be used to investigate the possible electric field distributions induced in tissues by far-field sources such as high-tension transmission lines. Moreover, the mechanism of charge build-up at interfaces between regions having different electrical conductivity clearly applies over a large range of length scales. For instance grey matter and white matter are themselves heterogeneous at a microscopic length scale and even at a finer sub-micron length scale of intracellular structures, such as organelles, vesicles, neurofilaments, etc. Charge may build up transiently across membrane boundaries or structures that are oriented perpendicular to the local induced electric field, leading to transport of ions and charged molecules.

Finally, in cardiac tissue subject to a uniform electric field, discontinuities or strong gradients in the extracellular conductivity that are not accompanied by concomitant variations in intracellular conductivity could give rise to changes in transmembrane potential (Trayanova 1999, appendix B). This effect could help explain the physical basis of cardiac defibrillation using far-field stimulating electrodes.

Acknowledgments

This work was supported in part by the Intramural Program of the National Institutes of Child Health and Human Development, NIH. LC and RS gratefully acknowledges the financial support of the Foundation for Science and Technology (FCT), Portugal.

References

Basser P J 1993 Cable equation for a myelinated axon derived from its microstructure *Med. Biol. Eng. Comput.* (Suppl.) **31** S87–92

Basser P J 2004 Scaling laws for myelinated axons derived from an electrotonic core-conductor model *J. Integr. Neurosci.* **3** 227–44

Basser P J and Roth B J 1991 Stimulation of a myelinated nerve axon by electromagnetic induction *Med. Biol. Eng. Comput.* **29** 261–8

Baumann S B, Wozny D R, Kelly S K and Meno F M 1997 The electrical conductivity of human cerebrospinal fluid at body temperature *IEEE Trans. Biomed. Eng.* **44** 220–3

Branston N M and Tofts P S 1991 Analysis of the distribution of currents induced by a changing magnetic-field in a volume conductor *Phys. Med. Biol.* **36** 161–8

Eaton H 1992 Electric field induced in a spherical volume conductor from arbitrary coils: application to magnetic stimulation and MEG *Med. Biol. Eng. Comput.* **30** 433–40

Fang Z P and Mortimer J T 1991 A method to effect physiological recruitment order in electrically activated muscle *IEEE Trans. Biomed. Eng.* **38** 175–9

Haueisen J, Ramon C, Eiselt M, Brauer H and Nowak H 1997 Influence of tissue resistivities on neuromagnetic fields and electric potentials studied with a finite element model of the head *IEEE Trans. Biomed. Eng.* **44** 727–35

Heller L and van Hulsteyn D B 1992 Brain stimulation using electromagnetic sources: theoretical aspects *Biophys. J.* **63** 129–38

Holdefer R N, Sadleir R and Russell M J 2006 Predicted current densities in the brain during transcranial electrical stimulation *Clin. Neurophysiol.* **117** 1388–97

Hursh J B 1939 Conduction velocity and diameter of nerve fibers *Am. J. Physiol.* **127** 131–9

Jalinous R 1991 Technical and practical aspects of magnetic nerve stimulation *J. Clin. Neurophysiol.* **8** 10–25

Kammer T, Beck S, Thielscher A, Laubis-Herrmann U and Topka H 2001 Motor thresholds in humans: a transcranial magnetic stimulation study comparing different pulse waveforms, current directions and stimulator types *Clin. Neurophysiol.* **112** 250–8

Kobayashi M, Ueno S and Kurokawa T 1997 Importance of soft tissue inhomogeneity in magnetic peripheral nerve stimulation *Electroencephalogr. Clin. Neurophysiol.* **105** 406–13

Kowalski T, Silny J and Buchner H 2002 Current density threshold for the stimulation of neurons in the motor cortex area *Bioelectromagnetics* **23** 421–8

Lassek A M 1940 The human pyramidal tract: II. A numerical investigation of the Betz cells of the motor area *Arch. Neurol. Psychiatry* **44** 718–24

Lassek A M 1942 The human pyramidal tract: IV. A study of the mature, myelinated fibers of the pyramid *J. Comp. Neurol.* **76** 217–25

Liu R and Ueno S 2000 Calculating the activation function of nerve excitation in inhomogeneous volume conductor during magnetic stimulation using the finite element method *IEEE Trans. Magn.* **36** 1796–9

Maccabee P J, Amassian V E, Eberle L P and Cracco R Q 1993 Magnetic coil stimulation of straight and bent amphibian and mammalian peripheral nerve *in vitro*: locus of excitation *J. Physiol.* **460** 201–19

Maccabee P J, Amassian V E, Eberle L P, Rudell A P, Cracco R Q, Lai K S and Somasundarum M 1991 Measurement of the electric field induced into inhomogeneous volume conductors by magnetic coils: application to human spinal neurogeometry *Electroencephalogr. Clin. Neurophysiol.* **81** 224–37

Mascagni M V and Sherman A S 1998 Numerical methods for neural modelling *Methods in Neuronal Modeling: From Ions to Networks* ed C Koch and I Segev (Cambridge, MA: MIT Press)

Miranda P C, Hallett M and Basser P J 2003 The electric field induced in the brain by magnetic stimulation: a 3D finite-element analysis of the effect of tissue heterogeneity and anisotropy *IEEE Trans. Biomed. Eng.* **50** 1074–85

Nagarajan S S and Durand D M 1996 A generalized cable equation for magnetic stimulation of axons *IEEE Trans. Biomed. Eng.* **43** 304–12

Nagarajan S S, Durand D M and Warman E N 1993 Effects of induced electric fields on finite neuronal structures: a simulation study *IEEE Trans. Biomed. Eng.* **40** 1175–88

Plonsey R and Barr R C 2000 *Bioelectricity: A Quantitative Approach* (New York: Kluwer Academic)

Rattay F 1986 Analysis of models for external stimulation of axons *IEEE Trans. Biomed. Eng.* **33** 974–7

Reilly J P 1989 Peripheral nerve stimulation by induced electric currents: exposure to time-varying magnetic fields *Med. Biol. Eng. Comput.* **27** 101–10

Rohan M, Parow A, Stoll A L, Demopulos C, Friedman S, Dager S, Hennen J, Cohen B M and Renshaw P F 2004 Low-field magnetic stimulation in bipolar depression using an MRI-based stimulator *Am J. Psychiatry* **161** 93–8

Roth B J 1994 Mechanisms for electrical stimulation of excitable tissue *Crit. Rev. Biomed. Eng.* **22** 253–305

Roth B J and Basser P J 1990 A model of the stimulation of a nerve fiber by electromagnetic induction *IEEE Trans. Biomed. Eng.* **37** 588–97

Roth B J, Cohen L G and Hallett M 1991a The electric field induced during magnetic stimulation *Electroencephalogr. Clin. Neurophysiol.* (Suppl.) **43** 268–78

Roth B J, Saypol J M, Hallett M and Cohen L G 1991b A theoretical calculation of the electric field induced in the cortex during magnetic stimulation *Electroencephalogr. Clin. Neurophysiol.* **81** 47–56

Rush S and Driscoll D A 1969 EEG electrode sensitivity—an application of reciprocity *IEEE Trans. Biomed. Eng.* **16** 15–22

Rushton W A H 1927 The effect upon the threshold for nervous excitation of the length of nerve exposed, and the angle between current and nerve *J. Physiol.* **63** 357–77

Schmid U D, Moller A R and Schmid J 1992 Transcranial magnetic stimulation of the facial nerve: intraoperative study on the effect of stimulus parameters on the excitation site in man *Muscle Nerve* **15** 829–36

Thielscher A and Kammer T 2002 Linking physics with physiology in TMS: a sphere field model to determine the cortical stimulation site in TMS *Neuroimage* **17** 1117–30

Tofts P S 1990 The distribution of induced currents in magnetic stimulation of the nervous system *Phys. Med. Biol.* **35** 1119–28

Tranchina D and Nicholson C 1986 A model for the polarization of neurons by extrinsically applied electric fields *Biophys. J.* **50** 1139–56

Trayanova N 1999 Far-field stimulation of cardiac tissue *Herzschr. Elektrophys.* **10** 137–48

Tuch D S, Wedeen V J, Dale A M, George J S and Belliveau J W 2001 Conductivity tensor mapping of the human brain using diffusion tensor MRI *Proc. Natl. Acad. Sci. USA* **98** 11697–701

Warman E N, Grill W M and Durand D 1992 Modeling the effects of electric fields on nerve fibers: determination of excitation thresholds *IEEE Trans. Biomed. Eng.* **39** 1244–54

Wolters C H, Anwander A, Tricoche X, Weinstein D, Koch M A and Macleod R S 2006 Influence of tissue conductivity anisotropy on EEG/MEG field and return current computation in a realistic head model: a simulation and visualization study using high-resolution finite element modeling *Neuroimage* **30** 813–26